Novel Active-Passive Two-Way Ranging Protocols for UWB Positioning Systems

Taavi Laadung, *Student Member, IEEE*, Sander Ulp, Muhammad Mahtab Alam, *Senior Member, IEEE*, and Yannick Le Moullec, *Senior Member, IEEE*

I. Introduction

Comparing previous [1] and more recent [2] survey articles covering various indoor positioning systems shows that in recent years the research interest in Ultra-Wideband (UWB) based indoor positioning has grown. UWB is an attractive technology having low power consumption, high immunity to interference from other devices, ability to penetrate various obstacles, short pulse duration for increasing robustness to multipath, and providing localization accuracy up to decimeter level in indoor scenarios [3]. The level of interest in UWB positioning is also demonstrated by its various applications for industrial [4], emergency [5], soldiers and first responders [6], unmanned aerial vehicle (UAV) [7], sports [8], and sensor fusion [9] positioning and navigation, to name a few.

The possible methods for positioning in an UWB system include fingerprinting based on the channel impulse response or power delay profile, distance estimation via path loss on received signal strength indicator (RSSI) or by angle of arrival (AOA) estimation. Although in their own right these methods are sufficient for providing a position estimate, they have some downsides. As indicated in [10], fingerprinting is a time consuming method requiring building up a signal parameter database, which can change over time with the positioning area; the RSSI method is very susceptible to interference caused by multipath propagation; finally, AOA estimation requires nodes equipped with antenna arrays, which subsequently increases the size and cost of the devices.

The remaining and more attractive positioning methods for UWB are called 1) time of flight (TOF), which is also called time of arrival (TOA), and 2) time difference of arrival (TDOA). TOF makes use of the relationship between the distance travelled and the propagation time when knowing the propagation speed, while TDOA employs the differences of arrival times of an emitted signal [11]. Although TDOA enjoys a minimal impact to the traffic in the network, it in turn needs strict synchronization between anchors. Estimating the TOF via two-way ranging (TWR) methods allows removing stringent synchronization requirements between anchors while posing a drawback by increasing the air time, compared to TDOA [12]. This in turn lowers the achievable tag density and raises the energy consumption in TOA/TOF methods [13]. Although, theoretical analysis and simulations show that TOA/TOF and TDOA are identical in their positioning performance, some practical cases show the superiority of TOA/TOF methods [14]. Pascacio *et al.* found that among researchers of indoor positioning, the topic of TOA/TOF is quite more popular than TDOA, although the reasons of the popularity were not investigated [15]. In order to take advantage of the relaxed synchronization requirements of TWR methods, while reducing the air time and power consumption, the notion of passive ranging with TWR is introduced. These methods incorporating passive ranging essentially provide a middle ground between TOF and TDOA position estimation by utilizing the positive sides of TDOA and reducing the negative effects of TWR methods.

Fujiwara *et al.* proposed a TOF/TDOA hybrid positioning system based on UWB transceivers developed in [16]. The system utilized a combination of single-sided two-way ranging (SS-TWR) TOF measurement by an active anchor, and a TDOA measurement employing a passive anchor, calculating the second TOF value using the TDOA measurement. By setting a geometric constraint to the possible location of a tag, the positioning system was able to provide a position estimate with only 2 anchors, with which it enabled to also reduce the number of communication times compared to TOF systems. Sahinoglu and Gezici expanded on the system in [17], and introduced a combination of multiple active and passive nodes with a maximum likelihood estimator (MLE), providing improved accuracy at reduced number of transmissions compared to conventional TOF systems.

Horváth *et al.* proposed Passive Extended Asymmetric Double-Sided Two-Way Ranging (PE-ranging) in which they

This project has received funding from the European Union's Horizon 2020 Research and Innovation programme under grant agreement No 951867 and 668995. This research has also been supported in part by the European Regional Development Fund, Study IT in Estonia Grant, and Estonian Research Council under Grant PUT-PRG424.

T. Laadung is with OÜ Eliko Tehnoloogia Arenduskeskus, 12918, Tallinn, Estonia and Thomas Johann Seebeck Department of Electronics, Tallinn University of Technology, 12616, Tallinn, Estonia (e-mail: taavi.laadung@eliko.ee, taavi.laadung@taltech.ee).

S. Ulp is with OÜ Eliko Tehnoloogia Arenduskeskus, 12918, Tallinn, Estonia (e-mail: sander.ulp@eliko.ee).

M. M. Alam is with Thomas Johann Seebeck Department of Electronics, Tallinn University of Technology, 12616, Tallinn, Estonia (e-mail: muhammad.alam@taltech.ee).

Y. Le Moullec is with Thomas Johann Seebeck Department of Electronics, Tallinn University of Technology, 12616, Tallinn, Estonia (e-mail: yannick.lemoullec@taltech.ee).

Pre-print version of the paper that appears in IEEE Sensors Journal (Early Access), 13 November 2021.
DOI: 10.1109/JSEN.2021.3125570

combine passive ranging proposed by [18] with symmetrical double-sided two-way ranging (SDS-TWR) [19]. This combination allowed to increase the ranging accuracy compared to previous SS-TWR-based passive ranging at the expense of adding a packet to the active ranging sequence. In [20] the same authors replaced SDS-TWR with Alternative Double-Sided Two-Way Ranging (AltDS-TWR), to eliminate the response delay time constraint that exists in SDS-TWR.

Shah *et al.* present in [21] three methods of passive ranging coupled with active ranging. The three methods achieve similar ranging performance to previous methods with the same or lower air time occupancy depending on the initiator of the ranging. This and the previous methods mainly aimed to reduce the air time of ranging methods by introducing passive ranging, only occasionally improving ranging accuracy by presenting new active ranging schemes. Additionally, the concept of a single active anchor proposes a single failure point where the disruption in the communication between the active anchor and tag also renders the passive range estimations incorrect, or even worse – losing the range estimations of that sequence altogether.

The authors of [22] expanded and generalized on Shah *et al.*'s concept to include multiple active-passive anchors alongside the passive anchors, calling it Active-Passive Two-Way Ranging (AP-TWR). Introducing hybrid role active-passive anchors, which also listen in on other transmissions when they themselves are not transmitting. Simulations and experimental results showed that the proposed method allowed to flexibly increase ranging accuracy even higher than the active ranging method could, while still offer reduced air time occupancy. Additionally, the problem of the single failure point was remedied by introducing multiple active-passive anchors ranging with the tag. However the paper only focused on using SS-TWR as the active ranging method, without considering other methods to improve ranging accuracy.

This paper extends on the active-passive two-way ranging (AP-TWR) method proposed by us in [22] to include previously overlooked active methods SDS-TWR and AltDS-TWR to further improve the method's ranging performance. In addition to this AP-TWR method, we also propose a new calculation method for passive range estimations in conjunction with active methods SS-TWR, SDS-TWR and AltDS-TWR, providing a second active-passive TWR method. Both of the investigated AP-TWR methods allow to choose a combination of active-passive and passive-only anchors to improve ranging accuracy and air-time efficiency compared to an equivalent active ranging method.

The remainder of the article is organized as follows. Section II provides the theoretical part of the active ranging methods. The formulation of the proposed active-passive methods is given in Section III; in Section IV we explain the concept of the measurement matrix which assembles the results of active-passive ranging and is the basis of the ranging accuracy improvement. Section V explains the basis and presents the numerical simulation results. Finally, a conclusion is drawn in Section VII.

II. Active Ranging Methods

This section presents the time-based active ranging methods which are used in practical UWB based positioning systems. These methods calculate an estimate of the time of flight (TOF) between two nodes by utilizing two-way packet exchanges. The resulting time of flight estimates can be converted to physical distance estimates by using

$$\hat{s} = c \cdot \hat{t}, \tag{1}$$

where $\hat{s}$ is the distance estimate, $\hat{t}$ the TOF estimate and c is the speed of light.

A single range estimate is acquired by utilizing a specific ranging method between an anchor and a tag. This implies that the number of range estimates per tag is directly dependent on the number of anchors with which the tag communicates. This is critical for positioning, as at least three range estimates are needed for a position estimate [23]. Moreover, having a larger number of range estimates also allows to lower the location estimation noise [24].

Sang *et al.* analyzed the errors of single-sided (SS), symmetrical double-sided (SDS), asymmetrical double-sided (ADS) and alternative double-sided (AltDS) two-way ranging (TWR) methods in [25]. All stated active methods, excluding ADS-TWR, are considered in this paper. ADS-TWR was omitted since it requires the last response delay time to be zero, which is unattainable in practical systems [21].

A. Single-Sided Two-Way Ranging

The IEEE 802.15.4a is an amendment to the IEEE 802.15.4 standard which introduced additional physical layers, which enabled precise wireless ranging [26]. In the standard, one of the specified ranging methods was Single-Sided Two-Way Ranging (SS-TWR), on which Sahinoglu and Gezici gave an overview and analysis in [27].

The SS-TWR method provides a TOF estimate by exchanging two packets between nodes. The method is illustrated in Fig. 1, where node A begins the sequence by simultaneously activating a timer and transmitting a packet to node B, which propagates through the air for its time of flight of $t_{A\leftrightarrow B}$. Upon arrival, node B responds after its response delay time $t_{B,A}$, which can be interpreted as the time interval measured by B, communicating with A. After propagating again for $t_{A\leftrightarrow B}$, node A receives the response and stops its timer, providing the round-trip time $t_{A,B}$, interpreted as the time interval measured by A in communication with B.

Generally the response delay time of nodes (in this specific case $t_{B,A}$) is several orders of magnitude larger than the TOF $t_{A\leftrightarrow B}$ [28]. The dotted lines of the time axis in Fig. 1 are used to denote the differences of scale.

The TOF between nodes A and B, $t_{A\leftrightarrow B}$, can then be calculated by

$$t_{A\leftrightarrow B} = \frac{t_{A,B} - t_{B,A}}{2}. \tag{2}$$

B. Symmetrical Double-Sided Two-Way Ranging

IEEE 802.15.4a standard also specified, in addition to SS-TWR, a second ranging method called Symmetrical Double-Sided Two-Way Ranging (SDS-TWR). Compared to SS-TWR,

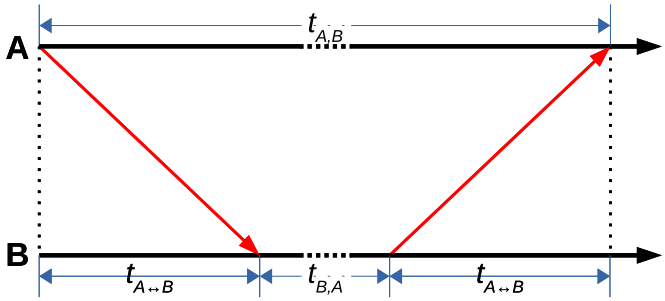

Fig. 1. Single-Sided Two-Way Ranging packet exchange.

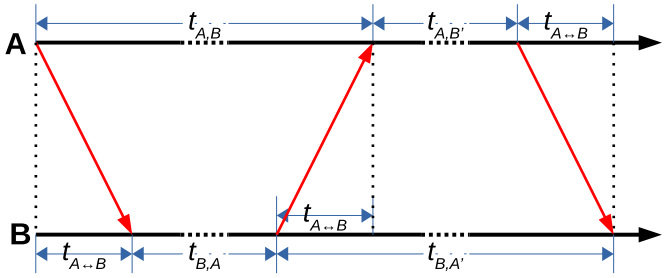

Fig. 2. Symmetrical- and Alternative Double-Sided Two-Way Ranging packet exchange.

SDS-TWR adds an additional packet to the ranging sequence. The introduction of the third packet to the ranging sequence allows to improve ranging accuracy [27], [28].

The packet exchange procedure for SDS-TWR is demonstrated in Fig. 2. As can be seen, the exchange of the first two packets is the same as in SS-TWR, discussed in Section II-A. After successfully receiving node B's response, node A transmits the third packet after its processing delay $t_{A,B'}$ (also interpreted as the second time interval measured by A when communicating with B). After propagating for $t_{A\leftrightarrow B}$, the final packet arrives at B, where the round-trip time of the last 2 packets, $t_{B,A'}$, is recorded.

Similarly to Fig. 1, the larger time scale of response delay times $t_{B,A}$ and $t_{A,B'}$ in Fig. 2 are illustrated by the dotted lines.

The four time intervals measured by nodes A and B can be used to estimate the TOF between them:

$$t_{A\leftrightarrow B} = \frac{t_{A,B} - t_{A,B'} + t_{B,A'} - t_{B,A}}{4}. \tag{3}$$

The error analysis of SDS-TWR presented in [25], [28] found that in order to minimize the TOF estimation error, A and B's response delays ($t_{B,A}$ and $t_{A,B'}$) have to be equal, hence the name symmetrical double-sided TWR. In a practical positioning system with multiple nodes it means that the final response packets to each node cannot be aggregated into a single response, raising the total number of packets in a ranging sequence. The effect on the air-time efficiency is further discussed in Section V-C.

C. Alternative Double-Sided Two-Way Ranging

The AltDS-TWR method utilizes the same exact packet exchange protocol as SDS-TWR, pictured in Fig. 2. The specifics of this protocol are discussed in the previous subsections.

The difference between SDS-TWR and AltDS-TWR becomes evident with the alternative derivation of the calculation of TOF proposed by Neirynck *et al.* in [28]:

$$t_{A\leftrightarrow B} = \frac{t_{A,B}\cdot t_{B,A'} - t_{A,B'}\cdot t_{B,A}}{2(t_{B,A} + t_{B,A'})} \tag{4a}$$

$$= \frac{t_{A,B}\cdot t_{B,A'} - t_{A,B'}\cdot t_{B,A}}{2(t_{A,B} + t_{A,B'})} \tag{4b}$$

$$= \frac{t_{A,B}\cdot t_{B,A'} - t_{A,B'}\cdot t_{B,A}}{t_{B,A} + t_{B,A'} + t_{A,B} + t_{A,B'}}. \tag{4c}$$

As a result, the four measured time intervals can be used to provide a TOF estimate in three distinct ways. The estimate can be calculated either by having node B's (4a), node A's (4b) or both nodes' (4c) measured time intervals in the denominator.

The error analysis of [25], [28] found that the alternative calculation of AltDS-TWR removes the symmetry constraint of response delays which hindered the SDS-TWR method. In a multiple-node system the dismissal of the symmetry constraint in turn allows to aggregate the final packets of node A to a single packet, reducing the total number of packets transmitted in a ranging sequence [29]. Additionally, using (4a) or (4b) permits to improve the TOF estimation performance if node B or node A has a better timing reference, respectively. If the nodes have clock sources with the same timing performance, the TOF estimate can also be obtained by (4c).

On account of offering the previously discussed improvement to SDS-TWR, AltDS-TWR has replaced it in the latest amendment to the IEEE 802.15.4 standard. The IEEE 802.15.4z amendment now specifies SS-TWR and AltDS-TWR as the main TOF-based ranging methods [30].

III. Proposed Active-Passive Ranging Methods

In this section we introduce two methods to provide ranging capabilities for passive anchors, which are also called listeners. Since the location of each anchor is fixed and known, the *a priori* information, in conjunction with information obtained during the ranging sequence, is used to passively provide estimates of distance between a listener and tag. The two proposed methods are collectively called the Active-Passive Two-Way Ranging (AP-TWR) due to the fact that the developed passive ranging capabilities are used in conjunction with existing active methods.

The proposed methods utilize a tag-initiated ranging sequence to provide the longest possible sleep time for the tag between consecutive ranging sequences. Employing an anchor-initiated ranging sequence was not considered, since the tag would have to be in a constant receive mode, which would reduce the tags battery life. For example, the widely used [31] Qorvo/Decawave DW1000 transceiver IC consumes more power during receiving than transmitting, let alone being asleep [32]. This constraint is introduced since tags are typically battery-operated and need to conserve power where possible.

This in turn means that an assumption is made i.e. anchors are not power-constrained, allowing them to remain in transmit or receive mode without sleeping between ranging sequences.

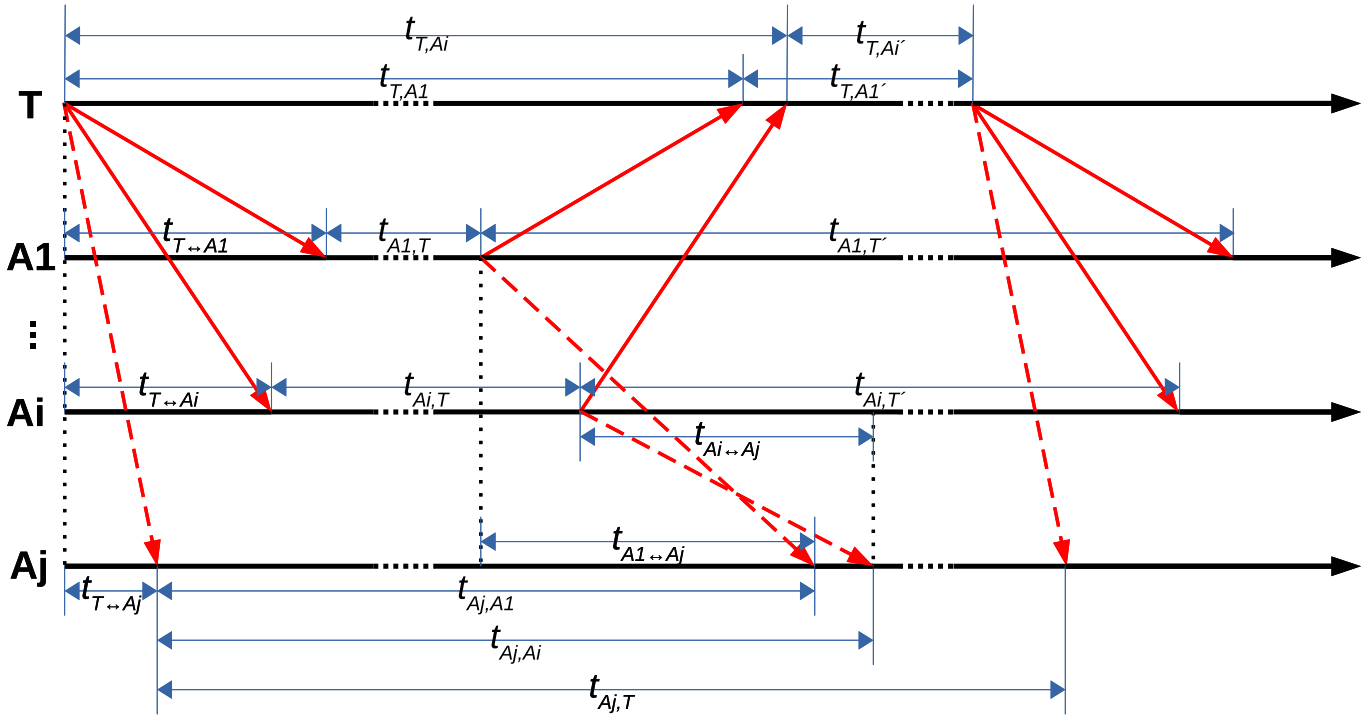

Fig. 3. A single ranging sequence for active-passive methods utilizing SS-TWR and AltDS-TWR with aggregated tag response. Tag T initiates the ranging sequence with a ranging request packet; anchors A1 to Ai receive it and answer with a ranging response. After receiving all responses, T ends the ranging sequence with a ranging report packet. Anchor Aj listens to all packet exchanges and records corresponding time intervals.

The notion is justified by the fact that generally anchors are a part of fixed infrastructure, having dedicated data and supply power lines, not running on batteries.

Since the anchors are not limited by supply power, it is practical to listen to every packet exchange that it receives, to provide additional information for ranging. This applies not only to the passive anchors, but to active anchors as well: when active anchors are not transmitting they can listen to transmissions between the tag and other active anchors. This allows for the distinction between active-passive and passive-only anchors.

In the scope of this paper the following abbreviations for system node names is adopted to help describe the principles of AP-TWR methods. Anchors numbered $1, 2, i$, which are actively participating in ranging, are abbreviated as A1, A2 and Ai, accordingly. The passive anchor is noted as Aj, and the tag as T.

A. Active-Passive Two-Way Ranging Method 1

This section proposes active-passive TWR method 1 (AP1-TWR), which exploits an active ranging method's packet exchange protocol alongside with knowledge about the anchor locations to provide passive range estimations alongside with active ranging results.

Fig. 3 represents a ranging sequence of AP-TWR methods utilizing SS-TWR and AltDS-TWR with aggregated tag report packet. Tag T starts the sequence with a ranging request, to which all active anchors A1 to Ai answer with a response. When T has received all responses, it ends the sequence with a broadcast ranging report packet which is received by each anchor. Passive anchor Aj listens in on the packet exchanges in the air and registers the corresponding time intervals of packet arrivals. Note that the final packet broadcast by T is an aggregated packet containing a response to all anchors; in this way T does not have to respond to each anchor individually so the effect on air time is reduced. This is discussed in more detail in Section V-C.

Fig. 4 gives the ranging sequence for AP-TWR methods utilizing the SDS-TWR. Although the packet exchange is similar to that of Fig. 3 for the first part of the sequence, the final responses sent by the tag are sent to individual anchors separately, to adhere to the response time symmetry constraint discussed in Section II-B. This means that the final response packets cannot be aggregated to a single one to reduce the air time.

The following notation of time intervals is used to describe the AP-TWR methods. The TOF between node A and B is represented by $t_{A\leftrightarrow B}$. Note that in Fig. 3 and 4 the TOFs are only labelled on the first packet but the same notation applies for TOFs in responses and in the report packet; this choice makes the figure less cluttered. The notation of $t_{A,B}$ is used to describe the time interval measured by node A, corresponding to packet exchange with node B. Since each active anchor measures two different time intervals associated with the same node, the distinction of the second time interval is made by adopting the notation $t_{A,B'}$.

The only differences between SS-TWR/AltDS-TWR and SDS-TWR based AP-TWR approaches is the notation of the listening anchor Aj's time intervals. In case of Fig. 3 depicting SS-TWR and AltDS-TWR based method, Aj records the time

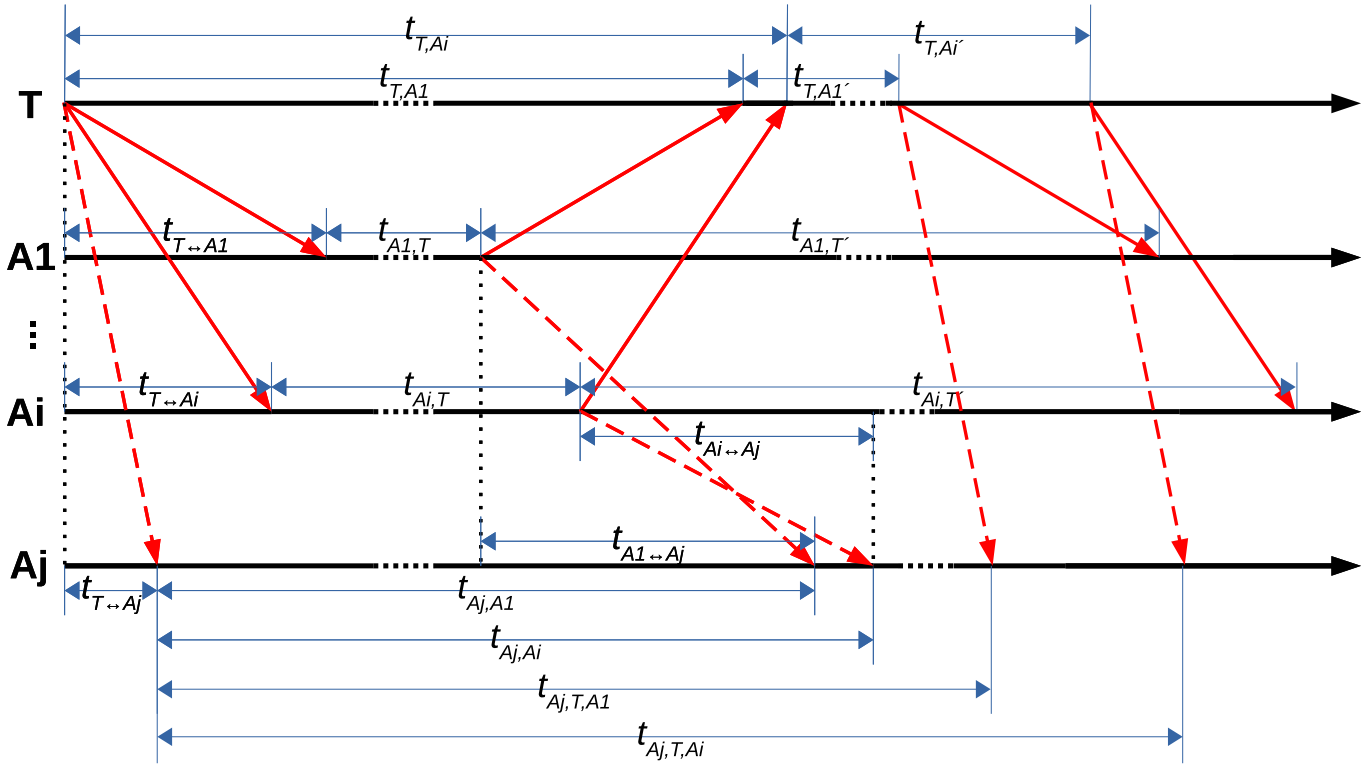

Fig. 4. A single ranging sequence for active-passive methods SDS-TWR without aggregated tag response. Tag T initiates the ranging sequence with a ranging request packet; anchors A1 to Ai receive it and answer with a ranging response. After receiving responses from the anchors, T transmits an anchor-specific report packet after delaying its response time equal to the anchor's processing time. Anchor Aj listens to all packet exchanges and records corresponding time intervals.

intervals corresponding to each active anchor ($t_{Aj,Ai}$), and the tag's final aggregated response $t_{Aj,T}$. For the SDS-TWR based approach, the final response packets are sent to each anchor separately, so Aj records the time intervals corresponding to each active anchor ($t_{Aj,Ai}$) plus the tag's response to each of the anchors ($t_{Aj,T,Ai}$).

Similar to active method, depicted in figures 1 and 2 and discussed in Section II, the time axis on Fig. 3 and 4 include the dotted lines to note time scale differences of tag and active anchor response delay times and the TOFs between nodes.

In order to have a generalized approach for AP1-TWR, we shall focus on the interaction between tag T, active anchor Ai and passive anchor Aj. It can be observed from both, Fig. 3 and Fig. 4 that the following time intervals are equal:

$$t_{T\leftrightarrow Ai} + t_{Ai,T} + t_{Ai\leftrightarrow Aj} = t_{T\leftrightarrow Aj} + t_{Aj,Ai}. \tag{5}$$

Rearranging (5) for $t_{T\leftrightarrow Aj}$ and adopting the notation of $t_{T\leftrightarrow Aj|Ai}$, we get

$$t_{T\leftrightarrow Aj|Ai} = t_{T\leftrightarrow Ai} + t_{Ai,T} + t_{Ai\leftrightarrow Aj} - t_{Aj,Ai} \tag{5a}$$

$$t_{T\leftrightarrow Aj|Ai} = t_{T\leftrightarrow Ai} + \tau_{Ai,1} - \tau_{Ai,0} + t_{Ai\leftrightarrow Aj} - \tau_{Aj,Ai} - \tau_{Aj,0}, \tag{5b}$$

where $t_{T\leftrightarrow Ai}$ is the TOF between T and Ai, estimated by an active ranging method, and $t_{Ai\leftrightarrow Aj}$ is the *a priori* known TOF from Ai to Aj. The rest of the terms in Eq. (5a) represent the calculation using the specific time intervals on Fig. 3, and Eq. (5b) presents the same calculation using timestamp notation as per Appendix B. The time interval notation of eq. (5a) can be used instead of the timestamp notation in eq. (5b), since the time base of each transmitting device can be converted to the time base of the receiver via Carrier Frequency Offset estimation method proposed by Dotlic *et al.* in [33]. This is further explained in Appendix B.

The notation of $t_{T\leftrightarrow Aj|Ai}$ is adopted instead of $t_{T\leftrightarrow Aj}$, to clarify that the TOF from tag T to listener Aj is calculated by using the data from active anchor Ai. This adaptation allows the calculation of TOF between tag T and listener Aj during each Ai's ranging session.

Since (5a) covers only the passive ranging results, the total set of ranging data acquired in a single ranging sequence can be expressed as:

$$t_{T\leftrightarrow Aj|Ai} = \begin{cases} t_{T\leftrightarrow Ai}, & \text{for } i = j \\ t_{T\leftrightarrow Ai} + t_{Ai,T} & \\ +t_{Ai\leftrightarrow Aj} - t_{Aj,Ai}, & \text{for } i \neq j, \end{cases} \tag{6}$$

where the first part corresponds to active ranging (since an anchor cannot listen to its own ranging session) and the second part to passive ranging using time interval notation. Note that the term $t_{T\leftrightarrow Ai}$ exists in both parts, meaning that the passive ranging is directly dependent on the active method with which the TOF is acquired.

Since active ranging can be utilized either by SS-TWR, SDS-TWR, or AltDS-TWR, the term $t_{T\leftrightarrow Ai}$ can be substituted

by (2), (3) or (4), respectively. The substitution provides three distinctive active-passive methods called AP1 SS-TWR, AP1 SDS-TWR and AP1 AltDS-TWR.

B. Active-Passive Two-Way Ranging Method 2

The second active-passive two-way ranging method (AP2-TWR) utilizes the same packet exchange sequence as AP1-TWR, but makes use of different measured time intervals to provide passive range estimations.

Fig. 3 illustrates the packet exchange protocol for AP2-TWR, and was already explained in detail in Section III-A. The figure allows us to observe that both of the following equalities hold:

$$t_{T\leftrightarrow Aj} + t_{Aj,Ai} = t_{T\leftrightarrow Ai} + t_{Ai,T} + t_{Ai\leftrightarrow Aj} \quad (7a)$$

$$t_{T\leftrightarrow Aj} + t_{T,Ai'} + t_{T\leftrightarrow Ai} = t_{Ai\leftrightarrow Aj} + t_{Aj,T} - t_{Aj,i}. \quad (7b)$$

Adding 7a to 7b, and solving for $t_{T\leftrightarrow Aj}$, we get the following expression:

$$t_{T\leftrightarrow Aj} = \frac{t_{Ai,T} + t_{Aj,T} - t_{T,Ai'}}{2} + t_{Ai\leftrightarrow Aj} - t_{Aj,Ai}. \quad (8)$$

According to Fig. 3 we know that $t_{Aj,T} = t_{T,Ai} + t_{T,Ai'}$. Substituting it into (8) and adopting the notation of $t_{T\leftrightarrow Aj|Ai}$ yields the final form for the passive part of AP2-TWR:

$$t_{T\leftrightarrow Aj|Ai} = \frac{t_{Ai,T} + t_{T,Ai}}{2} + t_{Ai\leftrightarrow Aj} - t_{Aj,Ai} \quad (8a)$$

$$t_{T\leftrightarrow Aj|Ai} = \frac{\tau_{Ai,1} - \tau_{Ai,0} + \tau_{T,Ai} - \tau_{T,0}}{2} + t_{Ai\leftrightarrow Aj} - \tau_{Aj,Ai} + \tau_{Aj,0}, \quad (8b)$$

where Eq. (8a) presents the AP2-TWR passive TOF estimate calculation via time interval notation, and Eq. (8b) with timestamp notation from Appendix B. The term $t_{Ai\leftrightarrow Aj}$ referring to the known TOF between Ai and Aj for both equations.

Similarly to Section III-A, this notation is introduced to emphasize that the TOF from passive anchor Aj to tag T can be calculated using every active anchor's ranging data. In addition, both time interval and timestamp notations are valid for the calculations, due to the possibility to translate the clock time bases between devices, explained in Appendix B.

The above proof applies to SS-TWR or AltDS-TWR based AP2-TWR methods, however we arrive to the same exact result using SDS-TWR as well. The proof for this is presented in Appendix A, where we show that utilizing the former and the latter methods for AP2-TWR, accordingly produce the same exact results in (8a) and (16).

Equations (8a) and (16) cover only the passive part of the ranging sequence. To define all the active and passive ranging data of a single ranging sequence, we express it as:

$$t_{T\leftrightarrow Aj|Ai} = \begin{cases} t_{T\leftrightarrow Ai}, & \text{for } i = j \\ \dfrac{t_{Ai,T} + t_{T,Ai}}{2} & \\ +t_{Ai\leftrightarrow Aj} - t_{Aj,Ai}, & \text{for } i \neq j, \end{cases} \quad (9)$$

where, again, the first part corresponds to an active ranging method and the second part corresponds to passive ranging with time interval notation. Similarly to III-A, the active ranging can be utilized either by SS-TWR, SDS-TWR, or AltDS-TWR, meaning that $t_{T\leftrightarrow Ai}$ can be substituted by (2), (3) or (4), respectively. This produces the active-passive methods AP2 SS-TWR, AP2 SDS-TWR and AP2 AltDS-TWR.

Although the main concept of AP2-TWR was already published in [22], that paper did not consider employing the SDS-TWR and AltDS-TWR methods. Only the effects of AP2 SS-TWR was simulated and shown to work in practical experiments.

IV. Measurement Matrix

After a ranging sequence has occurred, all the estimated TOF values of the AP-TWR methods can be expressed as an n by m measurement matrix T, where m is the number of active-passive anchors and n the total number of anchors, making the number of passive-only anchors as $k = n - m$:

$$T = \begin{bmatrix} t_{T\leftrightarrow A1|A1} & \dots & t_{T\leftrightarrow A1|Am} \\ \vdots & \ddots & \vdots \\ t_{T\leftrightarrow An|A1} & \dots & t_{T\leftrightarrow An|Am} \end{bmatrix}, \quad (10)$$

where, per (6) and (9), the active distance measurements lay on the main diagonal, and the passive measurements off the diagonal. T is an n by m matrix, meaning that we acquire a total of $n \cdot m$ raw range estimations for each ranging sequence, whereas an active-only method could only deliver m range estimations.

Each row of T contains the set of TOFs between an anchor and tag acquired during a ranging sequence. To express the coherence of these sets, we denote the rows of (10) as n vectors:

$$\boldsymbol{t_{T\leftrightarrow A1}} = \begin{bmatrix} t_{T\leftrightarrow A1|A1} & \dots & t_{T\leftrightarrow A1|Am} \end{bmatrix}$$

$$\vdots$$

$$\boldsymbol{t_{T\leftrightarrow An}} = \begin{bmatrix} t_{T\leftrightarrow An|A1} & \dots & t_{T\leftrightarrow An|Am} \end{bmatrix}.$$

Considering that each vector contains m estimates of the same TOF value, we can filter the noise by finding the mean value of each row vector, such that

$$\overline{T} = \begin{bmatrix} \overline{\boldsymbol{t_{T\leftrightarrow A1}}} \\ \vdots \\ \overline{\boldsymbol{t_{T\leftrightarrow An}}} \end{bmatrix}, \quad (11)$$

where $\overline{T}$ is a column vector containing n elements of filtered TOFs from tag to every anchor, effectively providing a set of range estimations as inputs for a positioning engine. This filtering takes place during each ranging sequence.

It is important to understand that for AP-TWR methods, as can be seen by the number of elements of (11), the total quantity of anchors n, directly defines the number of range estimates. At the same time, m only defines the cardinality of the row vectors of $\overline{T}$, affecting only the calculation of mean values in (11). On the other hand, active-only ranging methods with m range estimates do not offer the filtering of a single

ranging sequence's TOF values, the filtering can only be done with values of temporally consecutive ranging sequences.

V. Simulations and Results

In the following subsections we give the background of the simulation tool, present the preconditions, and compare the the simulated methods from the standpoint of range estimation root-mean-square-error (RMSE) and air-time efficiency.

A. Background and Conditions

In order to run the simulations for the proposed methods, a dedicated software tool was developed in R programming language. The software simulates all the required time intervals to calculate the various combinations of active and passive TOF estimates using (6) and (9).

Although the software does not simulate a full physical layer, the response times of each anchor are delayed separately to avoid collisions at the tag. Moreover, since only a single tag is simulated, a multiple access scheme for the tags is not implemented in the scope of this paper. Accounting these points, the events of packet loss are omitted from the simulations.

The simulations were carried out in a virtual room sized 500 cm x 700 cm x 250 cm. The combinations of AP-TWR methods were simulated for 1000 separate iterations. During each iteration, the tag and anchors were placed at randomly generated positions in the virtual room. Each iteration in turn consisted of 1000 separate ranging sequences.

In order to assess and compare the ranging performance of the methods, the range estimate RMSE is calculated using the following equation:

$$RMSE_d = \sqrt{\frac{\sum_{i=1}^{N}(d_i - d_t)^2}{N}}, \tag{12}$$

where d_i denotes the i-th range estimation, d_t the true range, and N the total number of range estimates.

The propagation conditions are set as line-of-sight, so the time measurement noise follows Gaussian distribution with a time measurement noise standard deviation of 150ps. The standard deviation is taken as the worst case scenario reported by McElroy *et al.* in [34] for Qorvo/Decawave DW1000.

Clock offset errors are omitted, since they can be compensated for, as Dotlic *et al.* proposed in [33]. All simulated nodes are assumed to have the same timing reference performance, meaning the 150ps standard deviation applies to both, the tag and anchors. Tag and anchor distance calibration errors are omitted, assuming that they are calibrated correctly.

The inter-anchor distances needed to calculate the passive range estimations are known and exact since anchors are assumed to be as a part of a fixed infrastructure with known locations (see Section III). Therefore, the inter-anchor TOFs can be found via the relation expressed by (1).

Each AP-TWR method utilized measurement matrix row-wise averaging by (11) to provide final TOF estimates. The TOF estimates were converted to distances using (1), to provide the final RMSE results in centimeters.

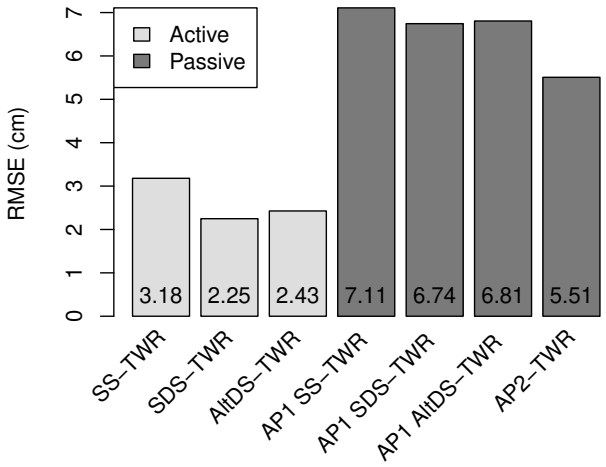

Fig. 5. Ranging performance of active and passive ranging methods.

Section III stated that both of the described AP-TWR methods can be used in conjunction with each of the active methods. Since in the scope of this paper, tag and anchors are assumed to have the same timing reference performance, we calculate AltDS-TWR method with (4c). As a total we simulate a combination of six active-passive methods: combining (6) and (9) with (2), (3), and (4c), we accordingly get AP1 and AP2 SS-TWR, AP1 and AP2 SDS-TWR, AP1 and AP2 AltDS-TWR.

B. Ranging Performance

In this section, the ranging performance of AP1 SS-TWR, AP1 SDS-TWR, AP1 AltDS-TWR, AP2 SS-TWR, AP2 SDS-TWR and AP2 AltDS-TWR is presented and discussed. The performance of these methods is compared in terms of range estimation RMSE in centimeters instead of TOF value, since distance is the final product of the ranging process in a practical sense.

Firstly, the individual performance of each active and passive method is observed separately. This is illustrated in Fig. 5, where the RMSEs of active methods SS-TWR, SDS-TWR, ADS-TWR, and passive parts of AP1 SS-TWR, AP1 SDS-TWR, AP1 AltDS-TWR and AP2-TWR methods are presented. Compared to AP1 methods, only a single combination of AP2-TWR is displayed, since this method is independent of the active ranging TOF estimation, as discussed in Section III.

The results show that at 2.25 cm RMSE, SDS-TWR has the best performance of all of the active methods, closely followed by 2.43 cm RMSE for AltDS-TWR; a bit further behind we find SS-TWR with 3.18 cm RMSE. Out of the passive methods we see that AP2-TWR performs the best with 5.51 cm RMSE, outperforming the next best, AP1 SDS-TWR, by a margin of 1.23 cm. Closely following it, we find AP1 ADS-TWR with

6.81 cm and last we find AP1 SS-TWR with an RMSE of 7.11 cm.

The individual results show that the best performance can be obtained using SDS-TWR for active ranging and AP2-TWR for passive ranging, while the least performing methods are SS-TWR and AP1 SS-TWR, respectively.

Fig. 6 presents the graphs of total system RMSE depending on the number of additional passive anchors, k, for each proposed active-passive method coupled with a measurement matrix averaging by (11). The individual graphs correspond to different values of m – the number of active-passive anchors. The methods are benchmarked against active-only SS-TWR, SDS-TWR and ADS-TWR methods, which are rendered as constant lines. They are depicted as constant lines since these methods do not provide passive ranging, they are therefore agnostic to the number of passive anchors.

The following trend for each method can be observed: system RMSE increases with each increment of the k value. This means that every additional passive range estimation value, which is supplied at no cost to the number of packets in a ranging sequence, contributes to an increase of the system RMSE. However, increasing m in turn decreases the system RMSE at the cost of an added packet in the ranging sequence. The impact of the method type and used anchor types on the air time is further discussed in Section V-C.

All AP2-TWR based methods outperform AP1-TWR based methods in every case of m, k value. For example from case $m = 3$ (Fig. 6 c) and upwards, AP2-TWR methods provide about 10 to 20 % decrease in RMSE when compared to AP1-TWR, depending on the specific case and method chosen. Cases below $m = 3$ still offer a decrease in RMSE, but the gain is less uniform across the graphs.

In both AP methods, it can be seen that employing AltDS-TWR and SDS-TWR active ranging methods yield almost identical RMSE, while also performing better than SS-TWR. It is important to note that the AP2 SS-TWR is inferior to AP2 SDS-TWR and AP2 AltDS-TWR by a slight margin of about 0.01 to 0.30 cm, which means all three AP2 methods provide almost the same performance. For AP1-TWR methods it can be seen that SS-TWR based method lags behind AltDS-TWR and SDS-TWR by a larger margin of about 0.10 to 0.50 cm. Aligning with the results of individual active and passive anchor performance, AP2 SDS-TWR and AP2 AltDS-TWR yield the lowest RMSE values while AP1 SS-TWR yield the highest ones, at every m, k value.

Fig. 6 c, $m = 3$ shows a breaking point where all the AP2-based active-passive methods have surpassed the ranging performance of active-only SS-TWR. Further increasing the number of active-passive anchors, we can see that all AP1-based active-passive methods achieve performance superior to active-only SS-TWR at $m = 5$. Accordingly for the same case, AP2-based methods have passed the performance of active AltDS-TWR. Case $m = 10$ illustrates that all the active-passive methods have surpassed every active-only method. Appendix C presents Fig. 10, where we can see that $m = 6$ is the critical value where all AP2-TWR methods catch up with the best performing active method SDS-TWR.

Table I presents an example case of AP2 SS-TWR compared to active-only SS-TWR. The example is constructed such that for both methods the total number of anchors is $n = m + k = 6$, where AP2 SS-TWR allows a total of six different active-passive and passive-only anchor m, k combinations. The results are compared to active-only SS-TWR which operates at 3.180 cm RMSE with 6 anchors. This specific case was selected since: 1) the amount of data to transmit is lower (refer to Section V-C); 2) according to Fig. 6, the RMSE cost of using AP2 SS-TWR instead of AP2 SDS or AP2 AltDS-TWR is only in the range of about 0.01 to 0.1 cm range; 3) the results are directly comparable to what was published in [22].

It is important to reiterate that the number of available range estimates for active methods is defined by the number of active anchors, but for AP methods it is dependent on the total number of anchors, as was discussed in Section IV. Additionally, all anchor combinations resulting $n < 3$ are unusable from the standpoint of positioning, since it was determined in Section I that providing a position estimate requires at least three range estimates. For the specific example drawn in Table I the number of available range estimates is 6 for all combinations.

The results show that depending on the m, k combinations, the RMSE of AP2 SS-TWR can increase up to 63.3% ($m = 1, k = 5$) or decrease down to -33.3% ($m = 6, k = 0$), compared to SS-TWR. Accordingly, while the air time is decreased by down to -62.5% or left unchanged at 0%. The table shows the critical point where jumping from 2 to 3 active-passive anchors in AP2 SS-TWR starts to provide constantly better RMSE results than active-only SS-TWR. The choice of m, k provides a flexibility to steer the system towards increased accuracy or decreased air time while providing the same number of range estimations. The intermediate cases and the interplay with air time efficiency is further discussed in Section V-C.

C. Air Time

blackThe air time efficiency of an UWB system can be assessed by two main categories: the amount of data to be transmitted over the air and the number of packets needed to transmit per each ranging sequence. The quantity of transmitted data directly impacts the effective length of the packet in bits, while a higher number of transmitted packets increases the total time spent transmitting in each ranging sequence.

Demanding applications where a large quantity of tags needs to be located simultaneously, the air-time efficiency and ranging rate may become a limiting factor to the maximum number of tags. Desirably both of the defining air time efficiency parameters should be kept to a minimum, since alongside with the ranging rate (frequency of consecutive ranging sequences), they dictate the maximum number of tags that can operate in a given area [13].

According to equations (3) and (4) in Sections II-B and II-C we see that in the case of ADS-TWR and AltDS-TWR the TOF from tag to anchor is calculated using four

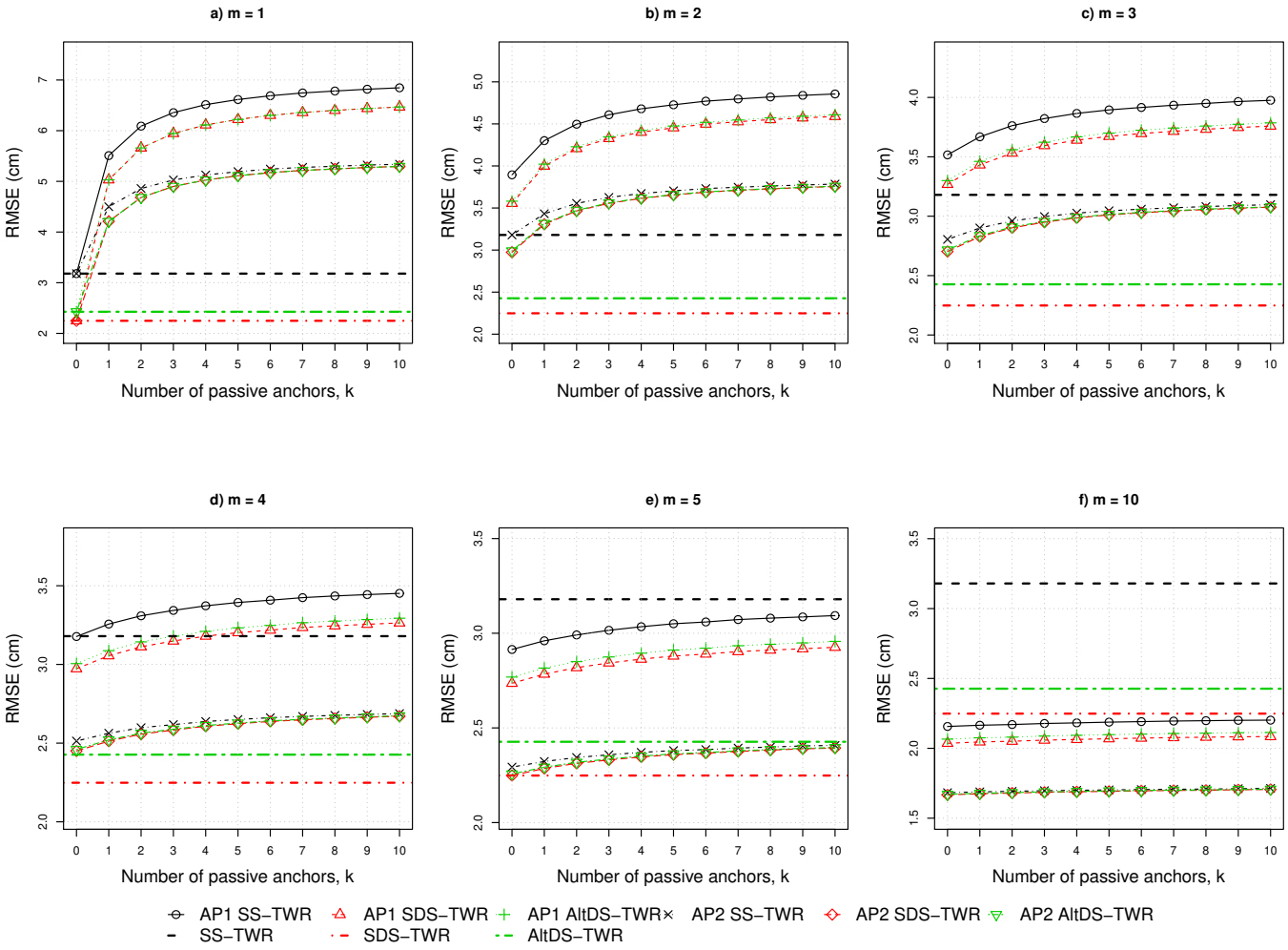

Fig. 6. Ranging performance of active-passive methods with measurement matrix averaging. The graphs are plotted to show each method's dependence of RMSE on n - the number of additional passive-only anchors. Each individual graph represents a different value for m - the number of active-passive anchors. The performance of active methods is pictured as constant lines, since they do not depend on number of passive anchors.

different variables. Two of these values are measured by the tag and need to be communicated back to the corresponding anchor. Since equation (2) for SS-TWR only needs a single time interval value from the tag to calculate the TOF, this effectively means that half as much information needs to be communicated back to corresponding anchors. This concept comes to play when the amount of transmitted data is limited or the shortest possible packet is desired. Since the spectrum is a shared resource, a shorter packet allows to increase the device density due to less time spent transmitting and resulting in a shorter protocol.

black Since the packets also contain varying length overhead in the form of preambles and headers etc., it is difficult to quantify the effect of transmitted data on the total length of a packet and therefore on the whole ranging sequence. Due to this, Fig. 7 only illustrates the total number of data fragments needed to communicate to anchors over the air, depending on the number of active anchors in a system. It can be seen that SS-TWR provides the lowest amount of data to be transmitted by the tag.

Furthermore, the second important part of air time efficiency is the number of packets in a ranging sequence. When considering a tag-initiated sequence with aggregated response as discussed in III and depicted in Fig. 3, the total number of packets in a sequence can be calculated as $N_a = m + 2$. Where N consists of a ranging request packet sent by the tag, m number of replies from each active anchor and an aggregated ranging report packet sent by the tag. The number of packets for a non-aggregated response would be calculated as $N_{na} = 2m + 1$, where the sequence consists of a ranging request sent by the tag, m responses from each active anchor and m ranging reports sent by the tag. In conclusion, the aggregated response packet saves us from transmitting $N_{na} - N_a = 2m+1-(m+2) = m-1$ packets. The described calculations of the number of packets in a sequence applies to both active-only and active-passive methods, depending only on the number of anchors actively taking part of the ranging.

It is important to reiterate the fact discussed in Section II-B that due to the response delay symmetry constraint the final packet of a SDS-TWR ranging session cannot be aggregated to a single one. This means that all methods (including AP-TWR methods) incorporating SDS-TWR

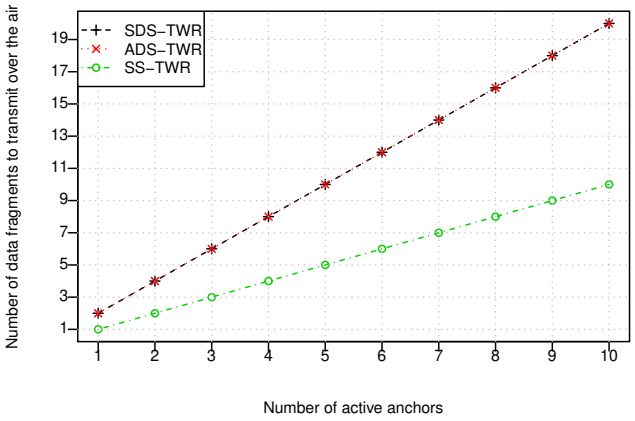

Fig. 7. Number of time interval values transmitted over the air by the tag, depending on the number of active anchors.

TABLE I
AP2 SS-TWR EXAMPLE, TOTAL NUMBER OF ANCHORS $n = m + k = 6$. COMPARED TO ACTIVE-ONLY SS-TWR WITH 6 ANCHORS (RMSE: 3.180 CM, NUMBER OF PACKETS IN RANGING SEQUENCE: 8). NUMBER OF AVAILABLE RANGE ESTIMATES: 6.

m	n	RMSE (cm)	RMSE relative change (%)	Nº packets	Air time relative change (%)
6	0	2.120	-33.3	8	0
5	1	2.323	-26.9	7	-12.5
4	2	2.598	-18.3	6	-25.0
3	3	2.997	-5.8	5	-37.5
2	4	3.672	15.5	4	-50.0
1	5	5.192	63.3	3	-62.5

transmit $N_{na} = 2m + 1$ packets in a single ranging sequence. Meaning SDS-TWR has a disadvantage of transmitting more packets in cases where $m > 1$.

The strengths of active-passive methods come to play with the addition of passive-only anchors. Passive-only anchors provide extra range estimates between themselves and the tag, while the number of packets in a ranging sequence is defined only by the number of active-passive anchors. This combats the main shortcoming of increased air time of TWR methods compared to TDOA methods, as discussed in Section I. Theoretically it would be possible to provide an unlimited amount of range estimates with only 3 packets in a ranging sequence when $m = 1$ and $k \longrightarrow \infty$, only limited by the number of physical anchor devices.

The example in Table I showed that depending on the m, k values in this case, the air time of AP2 SS-TWR can be decreased down to -62.5% compared to SS-TWR. The presented air time results are not only specific to AP2 SS-TWR: they also expand to other AP methods with aggregated packets with the same m, k values. This leaves out the methods which are based on SDS-TWR, since the relative air time change is calculated differently on the account of using unaggregated response packets.

Case $m = 6, k = 0$ the RMSE of ranging values is at its lowest with a -33.3% reduction compared to SS-TWR. The number of active-passive anchors is the same as the benchmark SS-TWR, at $m = 6$ with the number of transmitted packets at 8, giving no advantage of air time reduction. The other extreme case where $m = 1, k = 5$, the RMSE is at its highest of 5.192 cm with an increase of 63.3% compared to SS-TWR. This time the air time is at its lowest with 3 packets transmitted, giving an air time reduction of -62.5% compared to 8 packets transmitted in SS-TWR. The intermediate cases show that a middle ground where improvements for both parameters can be found. For example $m = 4, k = 2$ where both, the RMSE and air time, are decreased by -18.3% and -25%, respectively. Once again, the trends become obvious: each additional passive-only anchor increases the RMSE while the air time is decreased, and each additional active-passive anchor decreases the RMSE while adding a packet to the ranging sequence.

These results also align with the previous study placing our results between the simulation and experimental performance given in [22].

VI. EXPERIMENTAL RESULTS

The following section gives an overview of the practical experiments conducted. For the practical experiments the AP2 SS-TWR solution was selected as it requires the least amount of information and packets sent over the air and is comparable to the performance of the AP2 SDS-TWR and AP2 AltDS-TWR. The background information, experimental set up description and the results and analysis of the practical experiments utilizing AP2 SS-TWR are given in the following paragraphs. The results are analyzed from the standpoint of ranging performance.

A. Test Setup

The experiments took place at Tallinn University of Technology (TalTech), Thomas Johann Seebeck Department of Electronics. The tests were conducted using Eliko UWB RTLS [35], based on the Decawave/Qorvo DW1000 UWB transceiver. The test system composed of 5 anchors, a single tag.

The anchors and tag were placed in arbitrarily chosen locations in the U02-406 classroom at TalTech, making sure that a visual line of sight between all devices exists. This is illustrated on Fig. 8, where the anchors are marked with blue color and the tag marked with red.

The Leica DISTO S910 laser distance meter [36] was used to survey the true coordinates of the anchors and the tag relative to the front left corner of the classroom when entering it. The position of the laser distance meter is marked with yellow color in Fig. 8.

With 5 anchor network configuration the total number of possible m, k combinations is 15. Having 5 anchors to work with, made the total number of possible . For each combination 5 separate tests were performed to avoid outliers, and from each test 600 rangings were collected.

The captured ranging data packets in the form of text files were processed and analyzed using a dedicated software written in the programming language R.

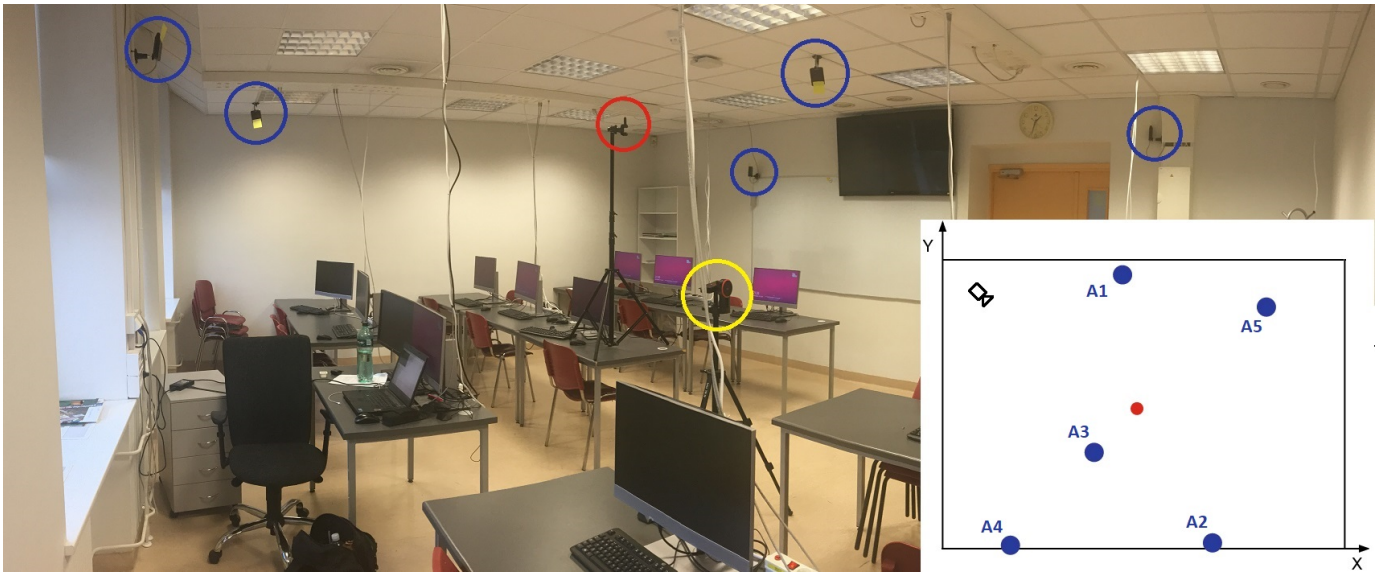

Fig. 8. The physical layout of the experimental setup. Anchors marked with blue, tag with red and the Leica DISTO S910 laser distance meter with yellow. The approximate location of taking the photograph marked with a camera symbol in the lower right hand corner schematic.

The practical performance of the AP2 SS-TWR was evaluated using σ, the standard deviation, as opposed to RMSE. This choice was made to eliminate the impact of device calibration errors and other static errors during measurements. The calculation of RMSE and standard deviation is similar: for RMSE the term d_t in (12) refers to the true distance, but in the calculation of standard deviation in (13) the term $\overline{d}$ is the mean value of all samples. This way the standard deviation reflects the best case RMSE value, assuming that the sample mean value is equal to the true distance:

$$\sigma_d = \sqrt{\frac{\sum_{i=1}^{N}(d_i - \overline{d})^2}{N}}. \tag{13}$$

It is also important to note that care was taken to monitor the sample mean values and the true distances to each anchor during all measurement sessions. This was done to verify that the practical measurement results conformed to real world anchor-tag distances, confirming that the method under test produces practically viable ranging results.

B. Experimental Results

This section presents the experimental results of AP2 SS-TWR, compares it with the performance attained in simulations and gives the analysis of said differences.

As also stated in the previous section, the practical results are presented as σ, the standard deviation of the measurements, which can be interpreted as the best-case RMSE value.

Table II presents the achieved AP2 SS-TWR method measurement standard deviation in centimeters for all allowed m, k combinations for a total number of $n = 5$ anchors. For the practical experiments, the baseline SS-TWR performance of case $m = 1, k = 0$ is taken as the average standard deviation of active ranging across the whole measurement campaign. In order to compare the experimental results, Table III presents the theoretical results for the same m, k combinations.

TABLE II
EXPERIMENTAL RESULTS: AP2 SS-TWR RANGING STANDARD DEVIATION (CM) FOR A MAXIMUM NUMBER OF $n = 5$ ANCHORS.

m \ k	0	1	2	3	4
1	2.475	3.742	4.408	5.068	5.287
2	2.929	3.005	3.058	3.132	
3	3.248	3.315	3.525		
4	3.583	3.708			
5	3.888				

TABLE III
SIMULATION RESULTS: AP2 SS-TWR RANGING RMSE (CM) FOR A MAXIMUM NUMBER OF $n = 5$ ANCHORS.

m \ k	0	1	2	3	4
1	3.180	4.500	4.858	5.027	5.192
2	3.180	3.432	3.555	3.626	
3	2.805	2.901	2.960		
4	2.513	2.563			
5	2.293				

The results and the main trends of the theoretical results were discussed in Section V-B. The following analysis focuses on the experimental results in Table II.

An overall trend can be observed, where the experimental results are comparable to the simulation results. Increasing the number of passive-only anchors k, the standard deviation of ranging results also increase.

The cases of $m = 1$ and $m = 2$ show that the practical AP2 SS-TWR functions better or similar compared to the simulation results, validating the method. The increased performance can be attained to the simulations assuming the worst case scenario for time measurement standard deviation discussed in Section V-A, while the practical system surpasses

this performance.

For cases where $m > 2$ the experimental results show higher standard deviation than the simulation results. The differences between the experimental and theoretical results are further discussed in the following paragraphs.

In order to analyze performance differences of the practical and simulated AP2 SS-TWR, two of the most notable cases were selected to illustrate the reasons. Based on Table II, the positive case of $m = 2, k = 3$ selected since the performance increased compared to previous $m = 1$ case, and the worst case of $m = 5, k = 0$ selected to reflect the worst overall performance.

TABLE IV
EXPERIMENTAL RESULTS. MEASUREMENT MATRIX STANDARD DEVIATIONS (CM) ACROSS ALL MEASUREMENTS FOR $m = 5, k = 0$. TRANSMITTING ANCHORS HEXADECIMAL IDS DEPICTED COLUMN WISE, LISTENING ANCHORS IDS ROW WISE, ACTIVE MEASUREMENTS ON MAIN DIAGONAL.

	A1	**A2**	**A3**	**A4**	**A5**
A1	2.412	6.288	6.888	6.787	8.011
A2	6.092	2.485	6.001	5.745	7.116
A3	6.482	6.032	3.165	6.472	7.472
A4	6.274	5.122	6.184	3.148	5.767
A5	5.896	6.136	5.785	4.715	4.071

Table IV represents the standard deviations in centimeters of the individual elements of the measurement matrix across all samples collected for case $m = 5, k = 0$. The column headers denote the transmitting anchor in the order of participating in the ranging sequence, while the row headers note the listening anchor. The standard deviation of each anchor's active measurement lays on the main diagonal.

TABLE V
EXPERIMENTAL RESULTS. MEASUREMENT MATRIX STANDARD DEVIATIONS (CM) ACROSS ALL MEASUREMENTS FOR $m = 2, k = 3$. TRANSMITTING ANCHOR DEPICTED COLUMN WISE, LISTENING ANCHORS ROW WISE, ACTIVE MEASUREMENTS ON MAIN DIAGONAL.

	A1	**A2**
A1	2.144	4.916
A2	5.012	2.490
A3	6.143	6.322
A4	5.690	5.943
A5	5.830	4.378

Similarly to Table IV, the standard deviations of the individual elements of the measurement matrix for case $m = 2, k = 3$ are presented in Table V, where again transmitting and listening anchors are displayed column and row wise, respectively.

Inspecting the active measurement standard deviations on the main diagonal of both of the tables, it can be seen that the values typically increase for each next active measurement in the ranging sequence. This is also confirmed by viewing the average standard deviation for active measurements of both cases: $m = 5, k = 0$ has 5 active measurements with an average standard deviation of 3.056 cm, while $m = 2, k = 3$ has a an average standard deviation of 2.317 across the 2 active measurements per ranging sequence. Comparing with the SS-TWR RMSE of 3.18 cm from Fig. 5, we observe that the the Eliko UWB RTLS offers better active ranging performance than simulations suggest.

Although the passive measurement standard deviations positioned off the main diagonal show slightly higher standard deviation compared to the simulated passive measurement RMSE of 5.51 cm stated on Fig. 5, there are some passive measurements that achieve better results. Among others achieving as low as 4.378 cm passive measurement standard deviation for anchor A5 listening on A2 in Table V.

On average, the standard deviation of passive measurements for $m = 5, k = 0$ is 6.263 cm and 5.530 cm for $m = 2, k = 3$. The former providing a higher standard deviation due to the higher errors in the final column of Table IV.

Overall, the standard deviations for measurements between practical and simulation results are comparable. The differences could be attributed to additional error sources from protocol timing errors, surrounding environment effects or device orientation propagation effects. For future work, the sources of errors could be researched and investigated.

VII. CONCLUSION

This article proposed an alternative calculation method for active-passive ranging and additionally expanded on the previous work done in [22] by including SDS-TWR and AltDS-TWR active methods with the proposed active-passive method, which was previously assessed only using SS-TWR. The proposed active-passive TWR methods called AP1 and AP2, respectively, were both paired with active ranging methods SS-TWR, SDS-TWR and AltDS-TWR. All of the six combinations of methods were validated by running simulations and comparing their range estimation RMSE and air time.

The results showed that all three AP2-TWR methods consistently outperform AP1-TWR methods by about 10 to 20%, depending on the chosen m, k. The SDS-TWR and AltDS-TWR variants perform almost identically, while exceeding SS-TWR's RMSE performance in both of the corresponding AP-TWR methods. Interestingly, depending on m, k values in AP2-TWR, the other active TWR variants outperform SS-TWR by only a maximum of 0.30 cm RMSE. Briefly, from the standpoint of range estimate RMSE, the best performing active-passive method is a tie between AP2 SDS-TWR and AP2 AltDS-TWR, with AP2 SS-TWR following very closely behind.

In addition to the range estimate RMSE, the amount of data needed to transmit and air time efficiency were also discussed as important performance indicators. It was found that in order to provide the shortest packet, i.e. the least amount of data needed to transmit from the tag, the SS-TWR is found to be most desirable requiring half as much data to be transmitted, compared to other active methods.

The air time efficiency was assessed as the number of packets exchanged in a ranging sequence. It was also found that in order to optimize the air-time efficiency for active TWR methods, an aggregated packet exchange protocol needs to be

employed. Out of all the methods, unfortunately, SDS-TWR is the only one that does not support packet aggregation due to its symmetrical response delay time requirement.

The air time efficiency can be further improved with the introduction of AP-TWR methods. The AP-TWR methods can provide the same amount of range estimations with less packets exchanged when compared to an equivalent active TWR method. As stated before, depending on the choice of m, k, the RMSE could be simultaneously lowered as well.

The AP2 SS-TWR method was chosen as a well-rounded example, offering a good balance between RMSE performance, number of transmitted data, and air time efficiency compared to other AP-TWR variants. Comparing it with an equivalent 6 anchor SS-TWR active method, the example $m = 4, k = 2$ showed a relative decrease of RMSE and air time by -18.3% and -25%, respectively. Sacrificing air time, the RMSE could be further reduced down to -33.3% ($m = 6, k = 0$); or vice-versa yield in RMSE, so the air time could be reduced down to -62.5% ($m = 1, k = 5$).

The practical experiments with AP2 SS-TWR verified the validity of the method and the results were comparable to the simulation results.

For future works, the practical performance of the other proposed active-passive methods could be evaluated. Additionally, the current practical experiments could be expanded and their performance assessed in non-line-of-sight conditions. Finally, the AP methods could be enhanced by additional measurement matrix analysis and processing to provide better performance and robustness of ranging.

APPENDIX A
PROOF FOR SDS-TWR BASED AP2-TWR

The SDS-TWR based AP2-TWR method on Fig. 4 allows us to observe that both of the following equalities hold:

$$t_{T\leftrightarrow Aj} + t_{Aj,Ai} = t_{T\leftrightarrow Ai} + t_{Ai,T} + t_{Ai\leftrightarrow Aj} \tag{14a}$$

$$t_{T\leftrightarrow Aj} + t_{T,Ai'} + t_{T\leftrightarrow Ai} = t_{Ai\leftrightarrow Aj} + t_{Aj,T,Ai} - t_{Aj,i}. \tag{14b}$$

Adding 14a to 14b, and solving for $t_{T\leftrightarrow Aj}$, we get the following expression:

$$t_{T\leftrightarrow Aj} = \frac{t_{Ai,T} + t_{Aj,T,Ai} - t_{T,Ai'}}{2} + t_{Ai\leftrightarrow Aj} - t_{Aj,Ai}. \tag{15}$$

According to Fig. 4 we know that $t_{Aj,T,Ai} = t_{T,Ai} + t_{T,Ai'}$. Substituting it into (15) and adopting the notation of $t_{T\leftrightarrow Aj|Ai}$ yields the final form for the SDS-TWR based AP2-TWR passive TOF estimate:

$$t_{T\leftrightarrow Aj|Ai} = \frac{t_{Ai,T} + t_{T,Ai}}{2} + t_{Ai\leftrightarrow Aj} - t_{Aj,Ai}. \tag{16}$$

Again, similarly to Section III-A, the notation of $t_{T\leftrightarrow Aj|Ai}$ is introduced to emphasize that the TOF from passive anchor Aj to tag T can be calculated using every active anchor's ranging data. It can also be seen that the final form of (16) is the same as (8a).

APPENDIX B
TIMESTAMPS IN AP-TWR

In the scope of this paper, the proof of AP-TWR methods is presented by using the notation of time intervals, as can be seen in Fig. 3. This notation is introduced to keep the intermediate equations concise. However, in practical transceivers such as the Qorvo/Decawave DW1000, on transmission or reception of an UWB frame each device returns a specific timestamp relative to its own internal counter instead of a time interval, marking that the devices have their own time base due to the clock offsets between them.

The Carrier Frequency Offset (CFO) estimation proposed by Dotlic *et al.* in [33] allows the clock offset values of a transmitter-receiver pair to be estimated, therefore the time base of the transmitter can be translated to the time base of the receiving device.

black This concept is illustrated on Fig. 9, in which the ranging sequence is identical to the one pictured on Fig. 3, differing only by the notation used in the time axes of the devices. The former utilizing the timestamp, and the latter resorting to time interval notation for the time axes of each device.

On Fig. 9, the timestamps are universally marked by τ, the disambiguation is made by the components presented in its subscript. The first component of the subscript marks the device which returns its current timestamps. For T and Aj, the second component marks the device the transmission originates from, and for A1 and Ai, the second component marks the number of the timestamp corresponding to packet exchange with T, since active anchors have two-way communication with the tag.

Comparing the notation of Fig. 3 and Fig. 9, it can be seen that a bijection between the two exists. This is further illustrated in Table VI, where in each row, a device's recorded time interval lengths on Fig. 3 is put into correspondence with the specific timestamps of Fig. 9. The bijection is valid if and only if the timestamps are in the same time base, which can be achieved using the aforementioned CFO estimation method.

Practical transceivers such as the DW1000 internally measure time in the form of timestamps [32]. In order to calculate range estimates they need to forward the measured time values as timestamp differences i.e. time intervals, so the conversions stated in Table VI need to be done in the devices. This is also the reason why the time interval notation is mainly used in the equations presented in this paper.

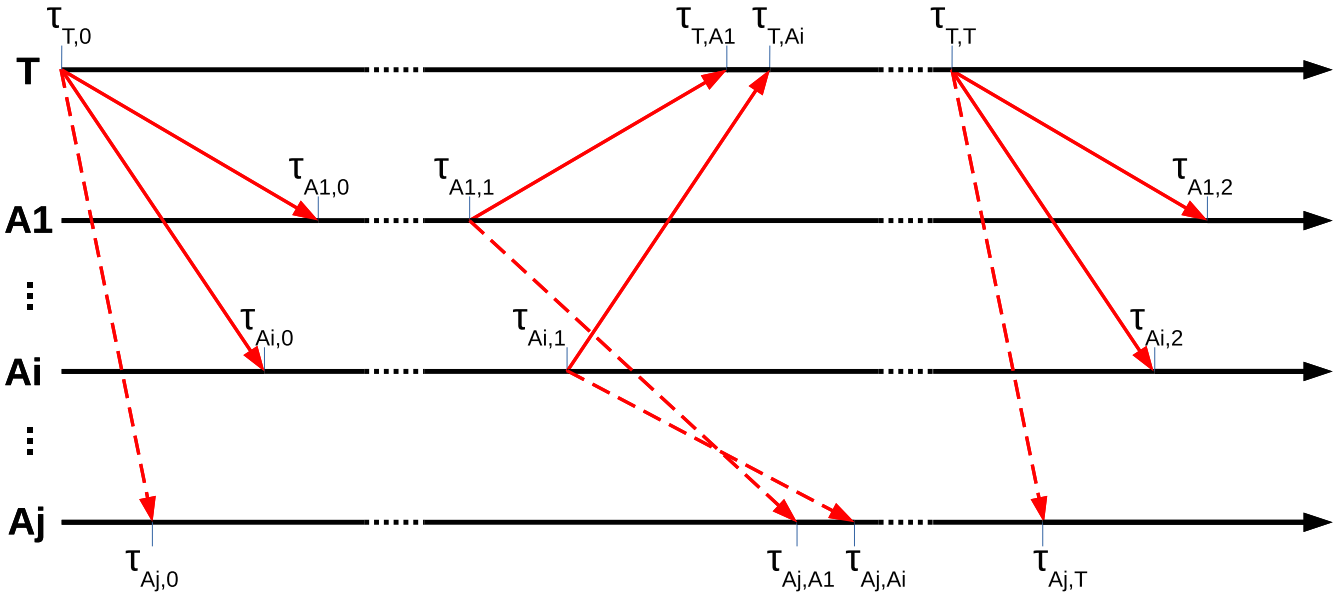

Fig. 9. Timestamps in SS-TWR and AltDS-TWR based active-passive methods. Each device records timestamps at packet transmission or reception times, relative to their local counter. These timestamp values can in turn be used to find the specific time intervals utilized in the proofs of AP-TWR methods proposed in this article.

TABLE VI
CORRESPONDENCE OF TIME INTERVAL NOTATION ON FIG. 3 TO THE TIMESTAMP NOTATION ON FIG. 9, DEPENDING ON THE SOURCE DEVICE.

Device	Correspondence			
T	$t_{T,A1} = \tau_{T,A1} - \tau_{T,0}$	$t_{T,A1'} = \tau_{T,T} - \tau_{T,A1}$	$t_{T,Ai} = \tau_{T,Ai} - \tau_{T,0}$	$t_{T,Ai'} = \tau_{T,T} - \tau_{T,Ai}$
Aj	$t_{Aj,A1} = \tau_{Aj,A1} - \tau_{Aj,0}$	$t_{Aj,Ai} = \tau_{Aj,Ai} - \tau_{Aj,0}$	$t_{Aj,T} = \tau_{Aj,T} - \tau_{Aj,0}$	
A1	$t_{A1,T} = \tau_{A1,1} - \tau_{A1,0}$	$t_{A1,T'} = \tau_{A1,2} - \tau_{A1,1}$		
Ai	$t_{Ai,T} = \tau_{Ai,1} - \tau_{Ai,0}$	$t_{Ai,T'} = \tau_{Ai,2} - \tau_{Ai,1}$		

APPENDIX C
ADDITIONAL SIMULATION RESULTS

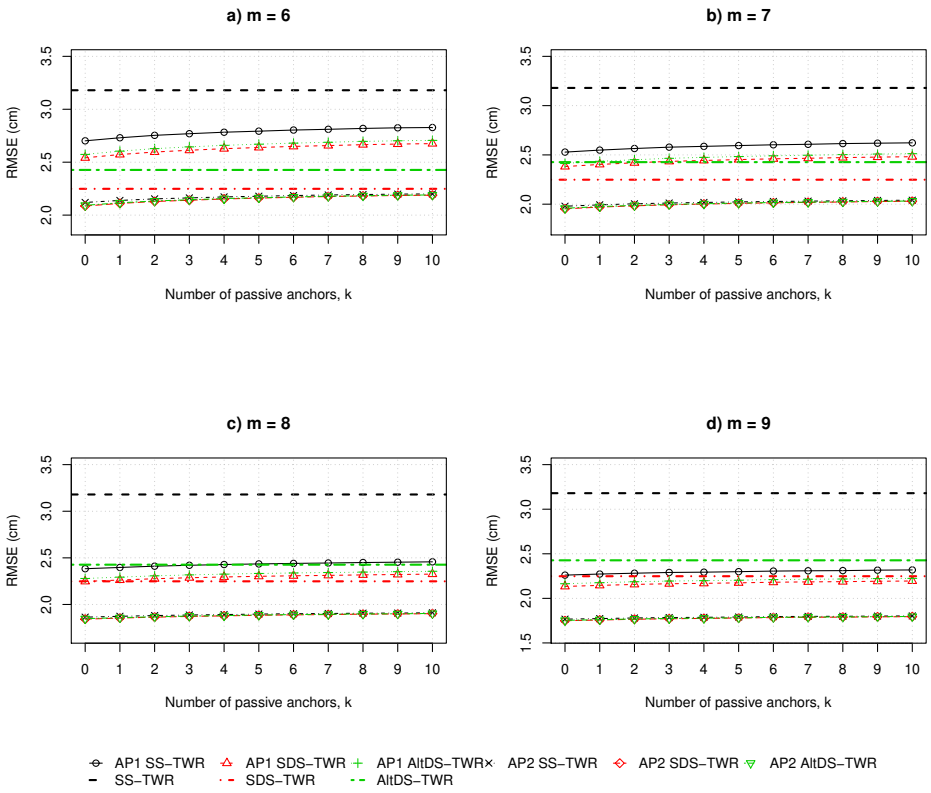

Fig. 10. Ranging performance of active-passive methods with measurement matrix averaging. Number of active-passive anchors $m = 6...9$.

REFERENCES

[1] G. Deak, K. Curran, and J. Condell, "A survey of active and passive indoor localisation systems," *Computer Communications*, vol. 35, no. 16, pp. 1939–1954, sep 2012.

[2] G. M. Mendoza-Silva, J. Torres-Sospedra, and J. Huerta, "A meta-review of indoor positioning systems," *Sensors (Switzerland)*, vol. 19, no. 20, 2019.

[3] F. Zafari, A. Gkelias, and K. K. Leung, "A Survey of Indoor Localization Systems and Technologies," *IEEE Communications Surveys & Tutorials*, vol. 21, no. 3, pp. 2568–2599, 2019.

[4] B. Silva, Z. Pang, J. Akerberg, J. Neander, and G. Hancke, "Experimental study of UWB-based high precision localization for industrial applications," in *2014 IEEE International Conference on Ultra-WideBand (ICUWB)*. IEEE, sep 2014, pp. 280–285.

[5] S. J. Ingram, D. Harmer, and M. Quinlan, "UltraWideBand indoor positioning systems and their use in emergencies," in *Record - IEEE PLANS, Position Location and Navigation Symposium*. IEEE, 2004, pp. 706–715.

[6] J. Rantakokko, J. Rydell, P. Strömbäck, P. Händel, J. Callmer, D. Törnqvist, F. Gustafsson, M. Jobs, and M. Grudén, "Accurate and reliable soldier and first responder indoor positioning: Multisensor systems and cooperative localization," *IEEE Wireless Communications*, vol. 18, no. 2, pp. 10–18, apr 2011.

[7] J. Tiemann, F. Schweikowski, and C. Wietfeld, "Design of an UWB indoor-positioning system for UAV navigation in GNSS-denied environments," in *2015 International Conference on Indoor Positioning and Indoor Navigation (IPIN)*. IEEE, oct 2015, pp. 1–7.

[8] M. Ridolfi, S. Vandermeeren, J. Defraye, H. Steendam, J. Gerlo, D. De Clercq, J. Hoebeke, and E. De Poorter, "Experimental Evaluation of UWB Indoor Positioning for Sport Postures," *Sensors*, vol. 18, no. 2, p. 168, jan 2018.

[9] D. Feng, C. Wang, C. He, Y. Zhuang, and X.-G. Xia, "Kalman-Filter-Based Integration of IMU and UWB for High-Accuracy Indoor Positioning and Navigation," *IEEE Internet of Things Journal*, vol. 7, no. 4, pp. 3133–3146, apr 2020.

[10] F. Mazhar, M. G. Khan, and B. Sällberg, "Precise Indoor Positioning Using UWB: A Review of Methods, Algorithms and Implementations," *Wireless Personal Communications*, vol. 97, no. 3, pp. 4467–4491, dec 2017.

[11] R. Zekavat and R. M. Buehrer, *Handbook of position location: Theory, practice and advances*. John Wiley & Sons, 2011, vol. 27.

[12] R. Zandian, "Ultra-wideband Based Indoor Localization of Mobile Nodes in ToA and TDoA Configurations," Ph.D. dissertation, University of Bielefeld, Germany, 2019.

[13] M. Ridolfi, S. van de Velde, H. Steendam, and E. De Poorter, "Analysis of the scalability of UWB indoor localization solutions for high user densities," *Sensors (Switzerland)*, vol. 18, no. 6, pp. 1–19, 2018.

[14] R. Kaune, "Accuracy studies for TDOA and TOA localization," *15th International Conference on Information Fusion, FUSION 2012*, pp. 408–415, 2012.

[15] P. Pascacio, S. Casteleyn, J. Torres-Sospedra, E. S. Lohan, and J. Nurmi, "Collaborative Indoor Positioning Systems: A Systematic Review," *Sensors*, vol. 21, no. 3, p. 1002, feb 2021.

[16] R. Fujiwara, K. Mizugaki, T. Nakagawa, D. Maeda, and M. Miyazaki, "TOA/TDOA hybrid relative positioning system using UWB-IR," in *2009 IEEE Radio and Wireless Symposium*. IEEE, jan 2009, pp. 679–682.

[17] Z. Sahinoglu and S. Gezici, "Enhanced Position Estimation via Node Cooperation," in *2010 IEEE International Conference on Communications*. IEEE, may 2010, pp. 1–6.

[18] M. R. Gholami, S. Gezici, M. Rydstrom, and E. G. Strom, "A distributed positioning algorithm for cooperative active and passive sensors," in *21st Annual IEEE International Symposium on Personal, Indoor and Mobile Radio Communications*. IEEE, sep 2010, pp. 1713–1718.

[19] K. A. Horvath, G. Ill, and A. Milankovich, "Passive extended double-sided two-way ranging algorithm for UWB positioning," in *International Conference on Ubiquitous and Future Networks, ICUFN*, 2017, pp. 482–487.

[20] K. A. Horvath, G. Ill, and A. Milankovich, "Passive extended double-sided two-way ranging with alternative calculation," in *2017 IEEE 17th International Conference on Ubiquitous Wireless Broadband, ICUWB 2017 - Proceedings*, 2017, pp. 1–5.

[21] S. Shah and T. Demeechai, "Multiple simultaneous ranging in IR-UWB networks," *Sensors (Switzerland)*, vol. 19, no. 24, pp. 1–14, 2019.

[22] T. Laadung, S. Ulp, M. M. Alam, and Y. Le Moullec, "Active-Passive Two-Way Ranging Using UWB," in *2020 14th International Conference on Signal Processing and Communication Systems (ICSPCS)*. IEEE, dec 2020, pp. 1–5.

[23] N. Lasla, A. Bachir, and M. Younis, "Area-based Vs. multilateration localization: A comparative study of estimated position error," in *2017 13th International Wireless Communications and Mobile Computing Conference (IWCMC)*. IEEE, jun 2017, pp. 1138–1143.

[24] G. Shen, R. Zetik, and R. S. Thomä, "Performance comparison of TOA and TDOA based location estimation algorithms in LOS environment," *5th Workshop on Positioning, Navigation and Communication 2008, WPNC'08*, vol. 2008, pp. 71–78, 2008.

[25] C. L. Sang, M. Adams, T. Hörmann, M. Hesse, M. Porrmann, and U. Rückert, "Numerical and experimental evaluation of error estimation for two-way ranging methods," *Sensors (Switzerland)*, vol. 19, no. 3, 2019.

[26] *Part 15.4: Wireless Medium Access Control (MAC) and Physical Layer (PHY) Specifications for Low-Rate Wireless Personal Area Networks (WPANs)*, IEEE Std., 2007.

[27] Z. Sahinoglu and S. Gezici, "Ranging in the IEEE 802.15.4a Standard," in *2006 IEEE Annual Wireless and Microwave Technology Conference*, vol. 128, no. 3330. IEEE, dec 2006, pp. 1–5.

[28] D. Neirynck, E. Luk, and M. McLaughlin, "An alternative double-sided two-way ranging method," in *Proceedings of the 2016 13th Workshop on Positioning, Navigation and Communication, WPNC 2016*, 2017, pp. 16–19.

[29] H. Kim, "Double-sided two-way ranging algorithm to reduce ranging time," *IEEE Communications Letters*, vol. 13, no. 7, pp. 486–488, jul 2009.

[30] *IEEE Standard for Low-Rate Wireless Networks–Amendment 1: Enhanced Ultra Wideband (UWB) Physical Layers (PHYs) and Associated Ranging Techniques*, IEEE Std., 2020.

[31] L. Flueratoru, S. Wehrli, M. Magno, and D. Niculescu, "On the Energy Consumption and Ranging Accuracy of Ultra-Wideband Physical Interfaces," in *GLOBECOM 2020 - 2020 IEEE Global Communications Conference*. IEEE, dec 2020, pp. 1–7.

[32] DW1000 User Manual V2.18. Decawave. Accessed March 28, 2021. [Online]. Available: https://www.decawave.com/dw1000/usermanual/

[33] I. Dotlic, A. Connell, and M. McLaughlin, "Ranging methods utilizing carrier frequency offset estimation," in *2018 15th Workshop on Positioning, Navigation and Communications, WPNC 2018*, no. 2. IEEE, 2018, pp. 1–6.

[34] C. McElroy, D. Neirynck, and M. McLaughlin, "Comparison of wireless clock synchronization algorithms for indoor location systems," in *2014 IEEE International Conference on Communications Workshops, ICC 2014*, 2014, pp. 157–162.

[35] Eliko Tehnoloogia Arenduskeskus OÜ. Eliko UWB RTLS. (2021, July 15). [Online]. Available: https://eliko.ee/uwb-rtls-ultra-wideband-real-time-location-system/

[36] Leica DISTO S910 User Manual. Leica Geosystems AG. Accessed July 16, 2021. [Online]. Available: https://shop.leica-geosystems.com/sites/default/files/2019-04/leica-disto-s910-user-manual-805080-808183-806677-en.pdf

Taavi Laadung (Student Member, IEEE) was born in Tallinn, Estonia in 1990. He received the B.Sc. and M.Sc. degrees in telecommunication from the Tallinn University of Technology, Tallinn, Estonia in 2013 and 2016, respectively. He is currently pursuing the Ph.D. degree in information and communication technology at Tallinn University of Technology. From 2015 to 2016, he was a course Practical Work Supervisor at Tallinn University of Technology. From 2017 to 2019, he worked in the Estonian Defence Forces as a Communication Systems R&D Specialist. Since 2019, he has been working as a Researcher at Eliko Tehnoloogia Arenduskeskus OÜ in Tallinn, Estonia. His research interests include the improving of algorithms and methods utilized in wireless indoor tracking, positioning and object locating systems.

Sander Ulp received the M.Sc. degree in telecommunication and the Ph.D. degree in information and communication technology from Tallinn University of Technology (TTÜ), in 2013 and 2019, respectively. From 2018 he started working as a researcher at Eliko Tehnoloogia Arenduskeskus OÜ. From 2019 he is the CTO of the competence center which develops novel indoor positioning research and technologies. His research interests are in distributed estimation, learning and adaptation over networks, digital signal processing, localization technologies, and indoor positioning.

Muhammad Mahtab Alam (Senior Member, IEEE) received the M.Sc. degree in electrical engineering from Aalborg University, Denmark, in 2007, and the Ph.D. degree in signal processing and telecommunication from the INRIA Research Center, University of Rennes 1, France, in 2013. He joined the Swedish College of Engineering and Technology, Pakistan, in 2013, as an Assistant Professor. He did his postdoctoral research at the Qatar Mobility Innovation Center, Qatar, from 2014 to 2016. In 2016, he joined as the European Research Area Chair holder and an Associate Professor with the Thomas Johann Seebeck Department of Electronics, Tallinn University of Technology, where he was elected as a Professor, in 2018. In 2019, he become the head of Communication Systems Research Group and leading number of National and International projects. His research interests include the fields of wireless communications and connectivity, NB-IoT 5G/B5G smart networks and services, and low-power wearable networks for SmartHealth.

Yannick Le Moullec (Senior Member, IEEE) received the M.Sc. degree from Université de Rennes I, France, in 1999, and the Ph.D. and HDR (accreditation to supervise research) degrees from Université de Bretagne Sud, France, in 2003 and 2016, respectively. From 2003 to 2013, he successively held Postdoctoral Researcher, Assistant Professor, and Associate Professor positions with the Department of Electronic Systems, Aalborg University, Denmark. He then joined Thomas Johann Seebeck Department of Electronics, Tallinn University of Technology, Estonia: Senior Researcher (2013 to 2016) and professorship (since 2017). His research interests include embedded systems, reconfigurable systems, the IoT, and the application thereof. He has supervised or co-supervised more than 50 M.Sc. students and 11 Ph.D. students. He has been involved in more than 20 projects, including five as PI, co-PI, or co-main applicant; one such notable project was the H2020 COEL ERA-Chair project from 2015 to 2019. He is an IEEE Senior Member, and a member of the IEEE Sustainable ICT Technical Community and of the IEEE Circuits and Systems Society.